한국전산구조공학회
1992년도 봄학술발표회 논문집

IMPLEMENTATION OF PSEUDODYNAMIC TEST METHOD

○ Waon-Ho Yi[1], Li-Hyung Lee[2], and Yong-Taeg Lee[3]

요 지

구조물의 비탄성 지진응답을 예측하기 위하여 수행되는 진동대 실험(Shaking Table Test)과 준정적 실험(Quasic-Static Test)의 각 장점을 조합한 유사동적 실험(Pseudodynamic Test)은 실물 크기 구조물의 비탄성 거동을 파악하는 데 널리 사용되고 있다. 이러한 유사동적 실험에서는 구조물에 변위이력의 정확한 가력 및 측정이 가장 중요하다. 측정된 변위와 계산된 변위의 차를 조절오차(Control Error)라고 하며, 임의의 단계에서 측정된 변위를 조정하므로서 그 다음 단계의 조절오차 및 측정오차(Measurement Error)를 감소시킬 수 있다. 따라서 개선된 유사동적 실험의 알고리즘을 얻을 수 있다.

1. Introduction

The main driving force for the development of the pseudodynamic test method has been the need for seismic performance data for large-scale structures. For a structure this size, shake-table tests would clearly be impractical. An additional advantage of the pseudodynamic test method is that it allows the test to proceed at a much slower rate than the earthquake. Thus more time is available to observe the accumulation of damage.

Of course, the pseudodynamic method also has some disadvantages: (1) the mass of the structure must be modeled mathematically; (2) deformation rate and stress relaxation effects can introduce errors in a test that proceeds slower than real life rate, and (3) the results can be very sensitive to measurement and control errors.

This paper deals with the last of these difficulties. Measurement and control errors tend to have a cumulative effect, and in some cases these have been seen to fully dominate the response. Particularly for MDOF systems there is a tendency for spurious excitation of the higher modes [Shing and Mahin (1983)].

2. Implementation of the Explicit Time Integration Scheme

Explicit time integration schemes include the central difference scheme, Newmark's method with $\beta=0$, and a modification of Newmark's Method [Shing and Mahin 1983]. There are different ways of implementing each of these methods for a pseudodynamic test.

These involve mainly the use of measured or computed displacements in the solution of the time-discretized equations of motion, and may lead to different error propagation characteristics. In this section attention is focused on the explicit Newmark method. The implementation of the method is explained by following the flow diagram in Fig. 1.

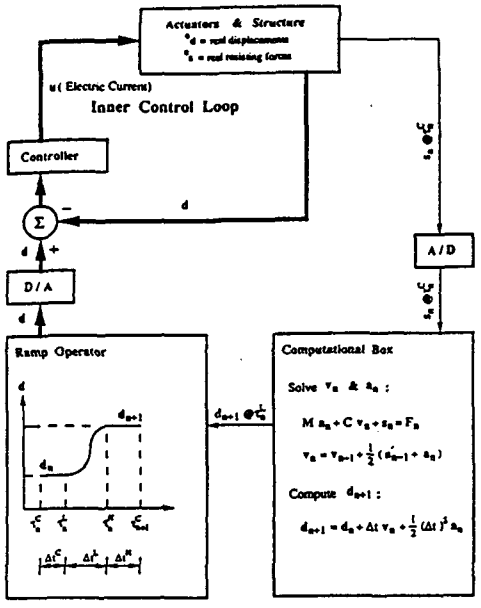

Fig. 1 Flow Diagram for Pseudodynamic Method Based on Explicit Scheme

1) Assistant Professor, Department of Architectural Engineering, Kwangwoon University
2) Professor, Department of Architectural Engineering, Hanyang University
3) Ph.D. Student, Department of Architectural Engineering, Hanyang University

Timestep n is taken to begin at time $\tau=\tau^C_n$ (*compute phase*) with the reading of the displacements and resisting forces, whose values after measurement and digitization errors are denoted by ${}^3d_n$ and ${}^3s_n$, respectively. The operations performed in the computational box are based on the following equations:

$$ {}^5s_n = {}^3s_n \tag{1} $$

$$ M\,{}^5a_n + C\,{}^5v_n + {}^5s_n = F_n \tag{2} $$

$$ {}^5v_n = {}^5v_{n-1} + \frac{\Delta t}{2}\,({}^5a_{n-1} + {}^5a_n) \tag{3} $$

$$ {}^5d_{n+1} = {}^5d_n + \Delta t\,{}^5v_n + \frac{1}{2}\,(\Delta t)^2\,{}^5a_n \tag{4} $$

$$ {}^6d_{n+1} = {}^6d_n + {}^5d_{n+1} - {}^3d_n \tag{5} $$

wherein the upper left index 5 (in ${}^5d_n$, ${}^5v_n$, ${}^5a_n$, and ${}^5s_n$) indicates values of the quantities that satisfy the time-discretized equations of motion, Eqs. 2-4. These will be referred to as the *consistent values* of the displacements, velocities, etc.
The computations proceed as follows:

1) The measured resisting forces will be used directly in the equations of motion as the consistent values. Hence Eq. 1.

2) Since the velocities and accelerations at time $n-1$ are available from the computations at the previous timestep, Eqs. 2 and 3 can be solved for the unknown velocities and accelerations at time n, ${}^5v_n$, and ${}^5a_n$.

3) The desired displacement for timestep $n+1$ is computed from Eq. 4.

4) In Eq. 5, the command signal for the displacement at timestep $n+1$ is computed as the sum of the command signal at the previous timestep plus a desired displacement increment. This desired displacement increment is the difference of the desired displacement for timestep $n+1$ and the measured displacement at timestep n.

The purpose of the compensation procedure in step 4 is to prevent the displacements that are actually imposed on the structure from drifting away from the desired displacements.

At the end of the compute phase, $\tau=\tau^L_n$ (*load phase*), the displacement command signal is incremented gradually from its value at time n to its value at time $n+1$, following a specified ramp function. This results in an out-of-balance voltage ${}^7d_n - {}^1d_n$ and produces the appropriate motion of the actuators. After a hold period, to allow the actuator motion to settle down, the resisting forces and displacements are again read, and the whole process is repeated with a unit increment in n.

3. Implementation of the Implicit Time Integration Scheme

The only difference in the hardware setup for the implicit scheme (see Fig. 2) lies in the use of force as well as displacement feedback in the inner control loop. The readings of the resisting forces used for control purposes are denoted ${}^1s$. These resisting forces are then multiplied by a matrix $\tilde{M}$, which will be defined later (Eq. 14). The resulting force feedback and the displacement feedback are summed to give an *adjusted predictor displacement*,

$$ {}^1\tilde{d} = {}^1d + \tilde{M}^{-1}\,{}^1s \tag{6} $$

The solution to the implicit time-discretized equations of motion for a timestep is reached when the adjusted predictor displacements reach a value that can be computed from

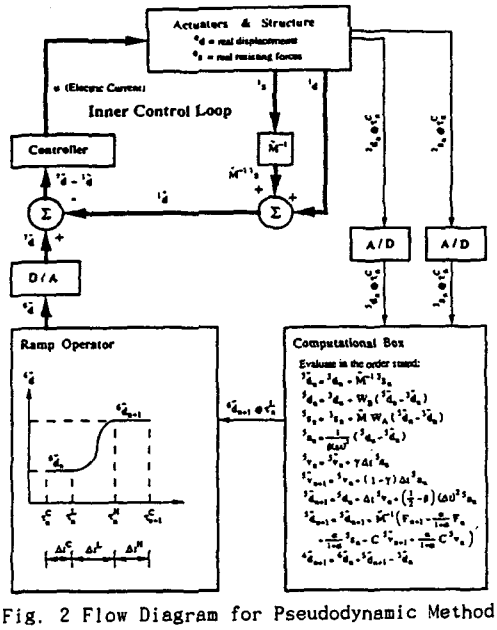

Fig. 2 Flow Diagram for Pseudodynamic Method Based on Implicit Scheme

information available from the solution at the previous timestep alone. Therefore the command signal for this case represents a set of adjusted predictor displacements. This command signal is varied gradually using a ramp function in exactly the same way as before.

The basic equations that describe the time integration scheme are:

$$Ma_{n+1} + (1+\alpha)Cv_{n+1} - \alpha Cv_n + (1+\alpha)s_{n+1} - \alpha s_n = (1+\alpha)F_{n+1} - \alpha F_n \quad (7)$$

$$v_{n+1} = \tilde{v}_{n+1} + \gamma \Delta t\, a_{n+1} \quad (8)$$

$$d_{n+1} = \tilde{d}_{n+1} + \beta(\Delta t)^2 a_{n+1} \quad (9)$$

where

$$\tilde{v}_{n+1} = v_n + (1-\gamma)\Delta t\, a_n \quad (10)$$

and

$$\tilde{d}_{n+1} = d_n + \Delta t\, v_n + \left(\frac{1}{2} - \beta\right)(\Delta t)^2 a_n \quad (11)$$

are the predictor values of the velocities and displacements. If the solution for timestep n is known, these predictor values can readily be computed. Thus Eqs. 7-9, together with the experimental force-displacement relation for timestep $n+1$,

$$s_{n+1} = s_{n+1}(d_{n+1}) \quad (12)$$

constitute the four equations that determine the solution for timestep $n+1$.

The unknown velocities and accelerations, v_{n+1} and a_{n+1} can be eliminated from Eqs. 7-9 to give:

$$d_{n+1} - \bar{d}_{n+1} + \tilde{M}^{-1} s_{n+1} = 0 \quad (13)$$

where

$$\tilde{M} = \frac{1}{(1+\alpha)\beta(\Delta t)^2} M + \frac{\gamma}{\beta \Delta t} C \quad (14)$$

and

$$\bar{d}_{n+1} = \tilde{d}_{n+1} + \tilde{M}^{-1}\left(F_{n+1} - \frac{\alpha}{1+\alpha} F_n + \frac{\alpha}{1+\alpha} s_n - C\tilde{v}_{n+1} + \frac{\alpha}{1+\alpha} Cv_n\right) \quad (15)$$

is the vector of adjusted predictor displacements for timestep $n+1$. Inspection of Eq. 15 reveals that these adjusted predictor displacements can be computed from the solution at timestep n alone. The problem at hand thus reduces solving Eq. 13 together with the experimental relation (Eq. 12) for unknowns d_{n+1} and s_{n+1}. This is exactly what is achieved by the inner loop actuator control circuit shown in Fig. 2: The command signal, produces actuator motion until the feedback, balances the command signal. At this point Eqs. 12 and 13 are satisfied, and Eqs. 8 and 9 can be solved for the unknown velocities and accelerations at time $n+1$. The resulting solution for timestep $n+1$ also must satisfy Eq. 7, since this equation can be recovered by substituting Eqs. 14 and 15 into Eq. 13.

As before, the timestep is taken to begin with the reading of the displacements and resisting forces at time $\tau=\tau^c{}_n$ (*compute phase*). As indicated in Fig. 2, the values of these quantities, after measurement and A/D conversion errors, are denoted ${}^3d_n$ and ${}^3s_n$, and calculated from Eq. 15. However, because of measurement and control errors, these quantities will not satisfy Eq. 13 exactly. Instead, the measured adjusted predictor displacements

$${}^3\bar{d}_n = {}^3d_n + \tilde{M}^{-1}\, {}^3s_n \quad (16)$$

differ from the computed or desired values of the adjusted predictor displacements. As before, it is convenient to define consistent values of the displacements, velocities, accelerations and resisting forces as those that satisfy the time-discretized equations of motion, Eqs. 7-9. Again these values are given an upper left index 5:

$${}^5\bar{d}_n - {}^5d_n + \tilde{M}^{-1}\, {}^5s_n = 0 \quad (17)$$

A number of possibilities present themselves for defining ${}^5d_n$ and ${}^5s_n$ such that Eq. 17 is satisfied. It will be seen that the choice will affect the error propagation characteristics of the method.

Possibility A: Use the measured displacements, and adjust the resisting forces;

$${}^5d_n = {}^3d_n \quad (18)$$

$${}^5s_n = -\tilde{M}\,({}^3d_n - {}^5\bar{d}_n) \quad (19)$$

Possibility B: Use the measured resisting forces, and adjust the displacements:

$${}^5s_n = {}^3s_n \quad (20)$$

$${}^5d_n = {}^5\bar{d}_n - \tilde{M}^{-1}\, {}^3s_n \quad (21)$$

Possibility C: Use a weighted average of possibilities A and B. In this case, the consistent values of the displacements and resisting forces are calculated from

$$ {}^5d_n = {}^3d_n + W_B({}^5\bar{d}_n - {}^3\bar{d}_n) \tag{22} $$

$$ {}^5s_n = {}^3s_n + \tilde{M}\, W_A({}^5\bar{d}_n - {}^3\bar{d}_n) \tag{23} $$

where weighting matrices, W_A and W_B must satisfy the condition

$$ W_A + W_B = I \tag{24} $$

where I is the identity matrix.

Once the consistent values of the displacements have been computed from Eqs. 22 and 23, the following expressions are evaluated in the order stated:

$$ {}^5a_n = \frac{1}{\beta(\Delta t)^2}\,({}^5d_n - {}^5\tilde{d}_n) \tag{25} $$

$$ {}^5v_n = {}^5\tilde{v}_n + \gamma\Delta t\ {}^5a_n \tag{26} $$

$$ {}^5\tilde{v}_{n+1} = {}^5v_n + (1-\gamma)\Delta t\ {}^5a_n \tag{27} $$

$$ {}^5\tilde{d}_{n+1} = {}^5d_n + \Delta t\,{}^5v_n + \left(\frac{1}{2} - \beta\right)(\Delta t)^2\ {}^5a_n \tag{28} $$

$$ {}^5\bar{d}_{n+1} = {}^5\tilde{d}_{n+1} + \tilde{M}^{-1}\left[F_{n+1} - \frac{\alpha}{1+\alpha}F_n + \frac{\alpha}{1+\alpha}\,{}^5s_n - C\,{}^5\tilde{v}_{n+1} + \frac{\alpha}{1+\alpha}C\,{}^5v_n\right] \tag{29} $$

$$ {}^6\bar{d}_{n+1} = {}^6\bar{d}_n + {}^5\bar{d}_{n+1} - {}^3\bar{d}_n \tag{30} $$

The new command signal is sent to the ramp operator box at time $\tau=\tau^L{}_n$ (*load phase*). From then on the procedure may be followed on the flow diagram in Fig. 2, and is analogous to the explicit case.

4. Error Analysis for the Explicit Time Integration Scheme

This section serves mainly as an introduction to the next, and to provide a basis for comparison of the error propagation characteristics of the explicit and implicit schemes.

As stated in Eqs. 2-4, the consistent values(upper left index 5) satisfy the time-discretized equations of motion. By taking the difference of each of Eqs. 2-4 and the corresponding equation for the unindexed quantities, it is seen that

$$ M\,{}^5a_{en} + C\,{}^5v_{en} + {}^5s_{en} = 0 \tag{31} $$

$$ {}^5v_{en} = {}^5v_{en-1} + \frac{\Delta t}{2}\,({}^5a_{en-1} + {}^5a_{en}) \tag{32} $$

$$ {}^5d_{en+1} = {}^5d_{en} + \Delta t\,{}^5v_{en} \frac{1}{2}(\Delta t)^2\ {}^5a_{en} \tag{33} $$

In other words, the cumulative errors of the consistent quantities satisfy the homogeneous time-discretized equations of motion. However, the consistent resisting forces are not the resisting forces corresponding to the consistent displacements. Indeed, for a nonlinear and history dependent structure, the resisting forces at timestep *n* in general depend on the displacements at each of the previous timesteps. Thus,

$$ s_n = s_n(d_1,\ d_2,\ d_3,\ \cdots\cdots,\ d_n) = s_n(D_n) \tag{34} $$

Assuming that the errors are small so that higher order terms in the errors can be neglected, Eq. 34 becomes:

$$ {}^0s_n = s_n + K_n\,{}^0p_{en} \tag{35} $$

$$ K_n = \frac{\partial s_n}{\partial D_n} = (K_{n1}\ K_{n2}\ \cdots\ K_{nn}),\ K_{mn} = \frac{\partial s_m}{\partial d_n} \tag{36} $$

Using the definitions and properties of the errors, Eq. 35 can be cast in the form

$$ {}^5s_{en} = K_n\,{}^5p_{en} + K_n\,{}^{50}p_{en} + {}^{05}s_{en} \tag{37} $$

$$ M\,{}^5a_{en} + C\,{}^5v_{en} + K_n\,{}^5p_{en} = f_n \tag{38} $$

$$ f_n = K_n\,{}^{05}p_{en} + {}^{50}s_{en} \tag{39} $$

In order to interpret the forcing function for the errors in terms of measurement and control errors, decompose the error terms on the right hand of Eq. 39, and use Eq. 1, to obtain

$$ f_n = K_n\,{}^{03}p_{en} + K_n\,{}^{35}p_{en} + {}^{30}s_{en} \tag{40} $$

5. Error Analysis for the Implicit Time Integration Scheme

By an argument entirely analogous to that for the explicit scheme, it can be shown that

$$ \begin{aligned} &M\,{}^5a_{en+1} + (1+\alpha)\,C\,{}^5v_{en+1} - \alpha\,C\,{}^5v_{en} \\ &+ (1+\alpha)\,K_{n+1}\,{}^5p_{en+1} - \alpha\,K_n\,{}^5p_{en} \\ &= (1+\alpha)\,f_{n+1} - \alpha\,f_n \end{aligned} \tag{41} $$

The decomposition of the terms in Eq. 39 is different for the implicit case. From Eqs. 22 and 23, it is seen that

$$ {}^{35}p_{en} = \tilde{W}_B\ {}^{35}\bar{p}_{en} \tag{42} $$

$$ {}^{35}s_{en} = \tilde{M}W_A\ {}^{35}\bar{a}_{en} \tag{43} $$

$$\bar{D}_n = \left[\bar{d}_1 \quad \bar{d}_2 \quad \bar{d}_3 \cdots \bar{d}_n \right]^T \qquad (44)$$

$\tilde{W}_B$ is a block diagonal matrix with n by n blocks in which the diagonal entries are the matrix W_B. Decomposing the error terms in Eq. 39 such that Eqs. 42 and 43 can be applied yields,

$$f_n = K_n {}^{03}D_{en} + K_n \tilde{W}_B {}^{35}D_{en} + M\tilde{W}_A {}^{53}\bar{d}_{en} + {}^{30}s_{en} \qquad (45)$$

If we consider a linearly elastic system with stiffness matrix K, and assume that there are no measurement errors, Eq. 45 reduces to

$$f_n = (KW_B - \tilde{M} W_A) \, {}^{35}\bar{d}_{en} \qquad (46)$$

If, in addition to being linearly elastic, the system considered has only one degree of freedom, the expression for the control errors (Eq. 45) reduces to

$$f_n = (W_B - \varkappa W_A) K \, {}^{35}\bar{d}_{en} \qquad (47)$$

in which

$$\varkappa = \frac{1}{4\pi^2(1+\alpha)\beta\left(\frac{\Delta t}{T}\right)^2} + \frac{\zeta\gamma}{\pi\beta\left(\frac{\Delta t}{T}\right)} \qquad (48)$$

and T and ζ are the natural period of oscillation and damping ratio of the system respectively. If possibility A is used, it is seen that the effect of the control errors increases very rapidly as Δt becomes small. This is similar to the phenomenon observed in the explicit scheme, when measured instead of computed displacements are used in the time integration scheme. On the other hand for possibility B, the error excitation function remains constant. Examination of Eq. 48 also reveals that the quantity $\varkappa$ can be interpreted as a cumulative error ratio, defined as the ratio of the absolute value of the effect of control errors for possibility A to that for possibility B. A plot of this error ratio as a function of the size of the timestep is given in Fig. 3. If there is no numerical or viscous damping $\alpha=\zeta=0$, the value of the error ratio is unity at the stability limit for central difference scheme ($\Delta t = T/\pi$), and increases like $1/(\Delta t)^2$ as the size of the timestep is decreased. Fig. 3 illustrates this behavior, and also reveals that the effect of numerical and/or viscous damping on the error ratio $\varkappa$ is relatively small. The values of the weighting factors for which the effect of control errors vanishes are

$$W_A = \frac{1}{1+\varkappa} \; ; \quad W_B = \frac{\varkappa}{1+\varkappa} \qquad (49)$$

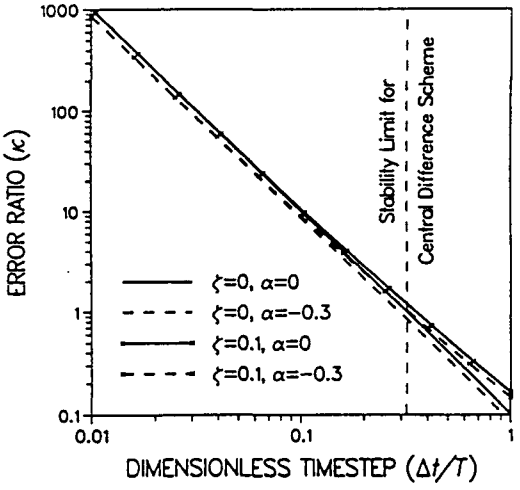

Fig. 3 Error Ratio for SDOF System

6. Conclusions

The error analysis presented herein hinges on the definition of what the authors refer to as consistent values of displacements, velocities, accelerations, and resisting forces as values of these quantities which satisfy the time-discretized equations of motion. (Due to experimental errors the consistent displacements and resisting forces do not exactly satisfy the force-displacement relation for the structure, however.) The error propagation characteristics of the method are seen to be strongly dependent on how these consistent values are obtained from the measured data: if the measured displacements are used to calculate these consistent values (Possibility A), the cumulative errors grow without bounds as the timestep is decreased. On the other hand, using the measured resisting forces to compute the consistent values (Possibility B) leads to more desirable error propagation characteristics.

If the structure is linearly eleastic and its stiffness matrix is known, it is possible to define the consistent values in such a way that the effect of control errors is eliminated completely. Although this cannot be achieved for a nonlinear and inelastic structure, the adjustment scheme can still be used to suppress the effect of control errors while the structure remains elastic.

REFERENCES

Hilber, H.M., Hughes, T.J.R., and Taylor, R.L., (1977), "Improved Numerical Dissipation for Time Integration Algorithms in Structural Dynamics," Earthquake Engineering and Structural Dynamics, Vol. 5, pp. 283-292.

Hilber, H.M., Hughes, T.J.R., and Taylor, R.L., (1978), "Collocation, Dissipation, and 'Overshoot' for Time Integration Schemes in Structural Dynamics," Earthquake Engineering and Structural Dynamics, Vol. 6, pp. 99-117.

Hughes, T.J.R., (1983), "Analysis of Transient Algorithms with Particular Reference to Stability Behavior," Chapter 2 in "Computational Methods for Transient Analysis," T. Belytschko and T.J.R. Hughes Editors, North-Holland Publishing Company.

Hughes, T.J.R., (1987), "The Finite Element Method, Linear Static and Dynamic Finite Element Analysis," p. 532, Prentice Hall, Inc.

Hughes, T.J.R., (1988), Pers. comm., June.

Kaminosono, T. et al., (1984), "U.S.-Japan Cooperative Research of R/C Full Scale Building Test. Part 1: Single Degree of Freedom Pseudo-Dynamic Test," Proceedings, Eighth World Conference on Earthquake Engineering, San Francisco, CA, July, Vol. 6, pp. 595-601.

McClamroch, H.N., (1985), "Displacement Control of Flexible Structures Using Electrohydraulic Servo-Actuators," Journal of Dynamic Systems, Measurement and Control, ASME, Vol. 107, March, pp. 34-39.

McClamroch, H.N. and Hanson, R.D., (1985), "Control Issues for Pseudodynamic Testing," Presented at the Second International Symposium on Structural Control, Waterloo, Ontario, Canada, July 16.

Newmark, M.N., (1959), "A Method of Computation for Structural Dynamics," Journal of the Engineering Mechanics Division, ASCE, No. EM3, Vol. 85, July.

Okamoto, S. et al., (1984), "U.S.-Japan Cooperative Research of R/C Full Scale Building Test. Part 2: Damage Aspects and Response Properties Before Repair Works," Proceedings, Eighth World Conference on Earthquake Engineering, San Francisco, CA, July, Vol. 6, pp. 603-610.

Shing, P.S.B. and Mahin, S.A., (1983), "Experimental Error Propagation in Pseudodynamic Testing," Earthquake Engineering Research Center, University of California, Berkeley, Report No. UCB/EERC-83/12, June.

Shing, P.S.B. and Mahin, S.A., (1987a), "Cumulative Experimental Errors in Pseudodynamic Tests," Earthquake Engineering & Structural Dynamics, Vol. 15, No. 4, pp. 409-424.

Shing, P.S.B. and Mahin, S.A., (1987b), "Elimination of Spurious Higher-Mode Response in Pseudodynamic Tests," Earthquake Engineering & Structural Dynamics, Vol. 15, No. 4, pp. 425-445.

Thewalt, C.A. and Mahin, S.A., (1987), "Hybrid Solution Techniques for Generalized Pseudodynamic Testing," University of California, Berkeley, Earthquake Engineering Research Institute, Report No. UCB/EERC-87/09, July.